RSC Advances

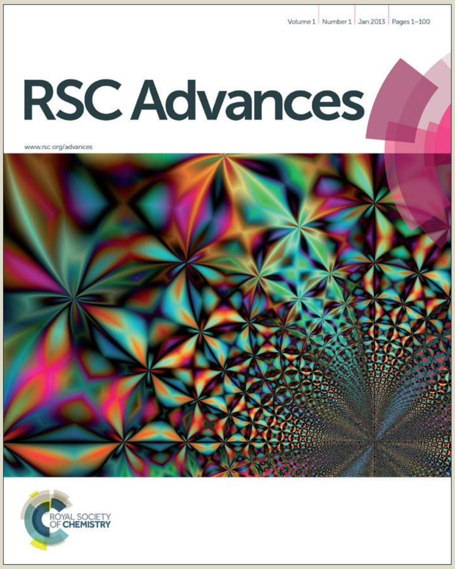
Volume 1 | Number 1 | Jan 2013 | Pages 1–100
RSC Advances
www.rsc.org/advances
ROYAL SOCIETY OF CHEMISTRY

This is an *Accepted Manuscript*, which has been through the Royal Society of Chemistry peer review process and has been accepted for publication.

Accepted Manuscripts are published online shortly after acceptance, before technical editing, formatting and proof reading. Using this free service, authors can make their results available to the community, in citable form, before we publish the edited article. This *Accepted Manuscript* will be replaced by the edited, formatted and paginated article as soon as this is available.

You can find more information about *Accepted Manuscripts* in the Information for Authors.

Please note that technical editing may introduce minor changes to the text and/or graphics, which may alter content. The journal's standard Terms & Conditions and the Ethical guidelines still apply. In no event shall the Royal Society of Chemistry be held responsible for any errors or omissions in this *Accepted Manuscript* or any consequences arising from the use of any information it contains.

ROYAL SOCIETY OF CHEMISTRY

www.rsc.org/advances

RSC Advances

www.rsc.org/xxxxxx

Dynamic Article Links ►

ARTICLE TYPE

Use of deuterium labelling – evidence of graphene hydrogenation by reduction of graphite oxide using aluminium in sodium hydroxide

Ondřej Jankovský[a], Petr Šimek[a], Michal Nováček[a], Jan Luxa[a], David Sedmidubský[a], Martin Pumera[b], Anna Macková[c,d], Romana Mikšová[c,d] and Zdeněk Sofer*[a]

Received (in XXX, XXX) Xth XXXXXXXXX 20XX, Accepted Xth XXXXXXXXX 20XX
DOI: 10.1039/b000000x

Highly hydrogenated graphenes are in the main focus of graphene research. Many unique properties of hydrogenated graphene are expected such as fluorescence, ferromagnetism, and tuneable band gap. The most widely used techniques for the fabrication of highly hydrogenated graphene are based on technically challenging methods concerning usage of liquid ammonia reduction pathway with alkali metals or plasma hydrogenation. On the other hand reduction of graphene oxide by nascent hydrogen is a simple and effective method leading to the formation of highly hydrogenated graphene at room temperature. We studied the hydrogenation of graphene oxides prepared by chlorate and permanganate methods by the deuterium labelling. The nascent hydrogen/deuterium was formed by the reaction of aluminum powder in the solution of sodium deuteroxide in deuterated water. The resulting hydrogenated graphenes were characterized in detail and the synthesis of highly hydrogenated graphenes was confirmed.

Introduction

After the discovery of graphene various chemical modifications of this layered material have been reported. [1] The most widely studied graphene derivatives are halogenated and hydrogenated graphenes.[2-5] Fully hydrogenated graphene with overall stoichiometry C_1H_1 is donated as graphane. Thanks to its outstanding physical and chemical properties graphane has attracted attention of scientists all around the world. [6] The band gap can be tuned by the content of hydrogen within the structure. While in graphene the bang gap value is 0 eV, in graphane the band gap increases to 3.7 eV. [7] The ferromagnetism and fluorescence of hydrogenated graphene were experimentally confirmed.[8, 9]

There are many routes to effective synthesis of hydrogenated graphene. The first one is the Birch reduction reaction, which involves introduction of solvated electrons into liquid ammonia and subsequent hydrogenation by proton sources such as alcohols. [10] The second procedure is based on low pressure hydrogenation using plasma [11] and the third one on high pressure hydrogenation of graphene or graphene oxides.[12] All these abovementioned methods require highly specialized equipment which may not be available. Moreover, relatively low levels of hydrogenation were observed using these methods.

In contrast, hydrogenation using nascent hydrogen is simple and effective. Graphite oxide can be reduced/hydrogenated at room temperature by hydrogen in atomic form which is usually formed by the decomposition of metals (Zn, Al, Mg, Mn and Fe) in an acidic solution. [13-16] Also the basic environment can be used for the evolution of hydrogen. Reduction of graphite oxide with Al / NaOH has been used for the synthesis of graphene-Al_2O_3 nanocomposites with outstanding transport properties. [17]

In this paper we prepared hydrogenated graphene by the reduction of graphite oxide by nascent hydrogen formed by reaction of sodium hydroxide with aluminum powder. In addition, we studied exact yield of hydrogenation using deuterium labeling followed by in-depth analysis by means of nuclear spectroscopic techniques (ERDA and RBS). The structure and composition of synthesized hydrogenated graphene was analyzed by SEM, EDS, STEM, high resolution XPS, Raman spectroscopy, combustion elemental analysis, FT-IR spectroscopy and resistivity measurement. We verified the applicability of nuclear spectroscopic method on analysis of graphene based materials. We will demonstrate that the deuterium labeling is highly useful for exact measurement of hydrogen concentration in the form of C-H bonds in hydrogenated graphenes.

Experimental

Materials

Graphite (2-15 µm, 99.9995%) was obtained from Alfa Aesar, Germany. Sulfuric acid (98 %), nitric acid (68 %), potassium chlorate (> 99%), potassium permanganate (99.5%), sodium nitrate (99.5%), hydrogen peroxide (30%), hydrochloric acid (37%), sodium hydroxide (98%), silver nitrate (> 99.8%) and barium nitrate (> 99%) were obtained from Penta, Czech Republic. Sodium (99%) and deuterium oxide (99.9%) was obtained from Sigma-Aldrich, Czech Republic. Aluminium

(99.7%, -325mesh) was obtained from Strem, USA. Deionized water (16.8 MΩ) was used for all syntheses. Argon (99.9996% purity) was supplied from SIAD, Czech Republic.

Synthesis

Graphite oxide prepared by chlorate route according to Hofmann method is termed as HO-GO.[18] The second graphite oxide was prepared by permanganate route according to Hummers method and it is denoted as HU-GO.[19] The synthesis procedure was entirely the same as in our previously published work.[20]

For the reduction 100 mg of graphite oxide was dispersed in 100 ml of 1 M solution of NaOH in H_2O and 1 M solution of NaOD in D_2O, respectively, by ultrasonication (400 W, 30 minute). NaOD was prepared by dissolving sodium in D_2O. Aluminum powder (1.5 g) was then added to the dispersion and the mixture was vigorously stirred for 24 hours. In the case of D_2O/NaOD the reduction was performed under argon atmosphere. Reduced graphene was separated by suction filtration and washed by diluted hydrochloric acid (1:10 by vol.) and deionized water. The product was dried in vacuum oven (60°C, 48 hours) prior the further use.

Characterization

Combustible elemental analysis (CHNS-O) was performed with a *PE 2400 Series II CHNS/O Analyzer* (Perkin Elmer, USA). In CHN operating mode, the most robust and interference free mode, the instrument employs a classical combustion principle to convert the sample elements to simple gases (CO_2, H_2O and N_2). The PE 2400 analyzer automatically performs combustion, reduction, homogenization, separation and detection of the gases. MX5 (Mettler Toledo) microbalance was used for precise sample weighing (1.5 – 2.5 mg per single sample analysis). The accuracy of CHN determination is better than 0.30 abs.% Internal calibration was performed using N-phenyl urea.

High resolution X-ray photoelectron spectroscopy (XPS) was performed on an *ESCAProbeP* (Omicron Nanotechnology Ltd, Germany) spectrometer equipped with a monochromatic aluminum X-ray radiation source (1486.7 eV). A wide-scan survey with subsequent high-resolution scans of the C 1s core level of all elements was performed. The relative sensitivity factors were used in the evaluation of the carbon-to-oxygen (C/O) ratios from the survey spectra. Samples were attached to a conductive carrier made from high purity silver bar.

Raman spectroscopy was carried out on *inVia Raman microscope* (Renishaw, England) with a CCD detector in backscattering geometry. Nd-YAG laser (532 nm, 50 mW) with 50x magnification objective was used for measurements. Instrument calibration was performed with a silicon reference which gives a peak centre at 520 cm^{-1} and a resolution of less than 1 cm^{-1}. In order to avoid radiation damage, laser power output used for this measurement was kept in a range of 0.5 mW to 5 mW. Prior to measurements, the samples were suspended in deionized water (concentration 1 mg/ml) and ultrasonicated for 5 minutes. Then the suspension was deposited on a small piece of silicon wafer and dried.

The morphology was investigated using scanning electron microscopy (SEM) with a FEG electron source (Tescan Lyra dual beam microscope). Elemental composition and mapping were performed using an energy dispersive spectroscopy (EDS) analyzer (X-Max^N) with a 20 mm^2 SDD detector (Oxford instruments) and AZtecEnergy software. To conduct the measurements, the samples were placed on a carbon conductive tape. SEM and SEM-EDS measurements were carried out using a 20 kV electron beam.

Fourier transform infrared spectroscopy (FTIR) measurements were performed on a NICOLET 6700 FTIR spectrometer (Thermo Scientific, USA). A Diamond ATR crystal and DTGS detector were used for all measurements, which were carried out in the range 4000–400 cm^{-1}.

The RBS and ERDA analysis was performed at tandem accelerator Tandetron 4130 MC. The RBS measurement was realized using 2 MeV He^+ ion beam and for the enhancement of detection sensitivity non-Rutherford back-scattering cross section at 3.716 MeV He^+ ions was used for nitrogen analysis. The incoming ion beam impinges the sample surface at 0° relative to the surface normal. Back-scattered ions were detected using ULTRA ORTEC detector placed below incoming beam (Cornell geometry) at the scattering angle 170°.

The ERDA measurement was performed using 2.5 MeV He^+ ions with the following geometry: 75° incoming ion beam angle and 30° scattering angle. Canberra PD-25-12-100 AM detector placed in plane with the incoming ion beam was used for the detection of forward scattered particles (H, D) and was covered by 12 μm Mylar foil for elimination of back-scattered He^+ ions.). The RBS and ERDA spectra were evaluated using the GISA 3.99 code and SIMNRA 6.06 codes [21-22], utilising cross-section data from IBANDL.[23]

To measure the electrical resistivity of the graphene, 40 mg was compressed into a capsule (¼ inch diameter) at a pressure of 400 MPa for 30 s. The resistivity of the capsules was measured by a four-point technique using van der Pauw method.[24] The resistivity measurements were performed with Keithley 6220 current source and Agilent 34970A data acquisition/switch control unit. The measuring current was set to 10 mA.

Electrochemical characterization was performed by cyclic voltammetry using Interface 1000 potentiostat (Gamry, USA) with a three-electrode set-up. The glassy carbon working electrode (GC), platinum auxiliary electrode (Pt) and Ag/AgCl reference electrode were obtained from Gamry (USA). For the cyclovoltammetric measurements, graphene was dispersed in DMF (1mg/ml) and 3 μl was evaporated on the glass carbon working electrode. All potentials referred in the following section were measured against the Ag/AgCl reference electrode. To measure the inherent electrochemistry, a phosphate buffer solution (PBS, 50 mM, pH=7.2) was used as the supporting electrolyte.

Results and discussion

Two different graphite oxides were reduced and hydrogenated by the nascent hydrogen which was formed by reaction of aluminum powder with NaOH/NaOD. Samples were termed according to graphite oxide precursor (HO-GO or HU-GO) and the used solutions (NaOH in H_2O or NaOD in D_2O) as 'HO-OH' 'HU-OH' 'HO-OD' and 'HU-OD'. For more details see the experimental section. The process is described in **Scheme 1**.

The morphology of reduced / hydrogenated graphenes is shown in **Figure 1**. The typical lamellar structure can be seen on all samples. The slight differences in the structure and morphology resulted from differences in starting graphite oxide, where for the graphene originating from HU-GO more wrinkled samples are observed. SEM-EDS measurements were performed to obtain information about the elemental composition. In addition to carbon and oxygen the traces of aluminium and sodium were detected as well. These impurities originated from the synthesis procedure. The precise composition is summarized in **Table I**.

Table 1 The results of SEM-EDS in at. %.

Sample	C	O	Na	Al
HO-OH	75.9	23.4	0.5	0.2
HO-OD	81.2	18.6	0.1	0.1
HU-OH	86.4	13.5	0.1	0.0
HU-OD	81.2	18.6	0.1	0.1

The composition and C/O ratio was measured using XPS. The survey spectra are shown in **Figure 2** where both carbon (C1s at ~284.5 eV) and oxygen peaks (C1s at ~532 eV) are clearly visible. The XPS spectra of starting graphite oxide are shown in Supporting Information (**Figure SI1**). The obtained concentrations of carbon, oxygen and C/O ratios are summarized in **Table 2**. The C/O ratios in the range of 6-7 were observed for all samples except for HU-OH sample with the ratio C/O = 3.8. Considering the C/O ratio in the starting graphite oxide was 2.3 and 2.4 for HU-GO and HO-GO, respectively, all resulting values are significantly higher compared to C/O ratios in the starting graphite oxide (~2) indicating a successful reduction of graphite oxide. Except for carbon and oxygen also traces of sodium (up to 0.3 at.%) were also detected. The small peak at ~370 eV can be attributed to silver holder. Since no other elements were detected, we can conclude that no impurities are present in an amount sufficient to trap some significant amount of deuterium or hydrogen, (such as $Al(OH)_3$ or $Al(OD)_3$) and the deuterium detected in the reduced graphene thus originates dominantly from the C-D bonds.

Table 2 The concentration of carbon and oxygen and C/O ratios obtained by XPS spectroscopy in atomic %.

Sample	C [at.%]	O [at.%]	C/O
HO-OH	87.2	12.8	6.8
HO-OD	86.3	13.7	6.3
HU-OH	79.0	21.0	3.8
HU-OD	87.5	12.5	7.0

High resolution XPS was also used for further investigation of carbon chemical environment and bonding characteristics of carbon atoms within graphene. The high resolution XPS spectra of C 1s peak are shown in **Figure 3**. The deconvolution of C 1s peak was performed to estimate the concentration of various functional groups bonded to the carbon atoms. Energies of C=C bond at 284.4 eV, C-C and C-H at 285.4 eV, C-O at 286.3 eV, C=O at 288 eV, O-C=O at 289 eV and π-π* interactions at 290.5 eV were considered for the deconvolution. The results are summarized in **Table 3** and can be compared with the results of C 1s peak deconvolution of starting graphite oxides given in Supporting Information (**Table SI A**).

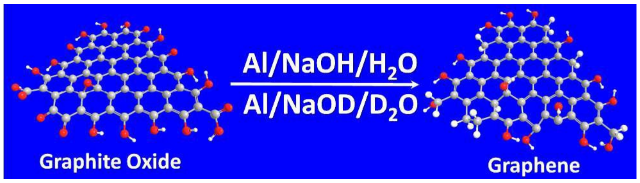

Scheme 1 Synthesis of hydrogenated graphenes

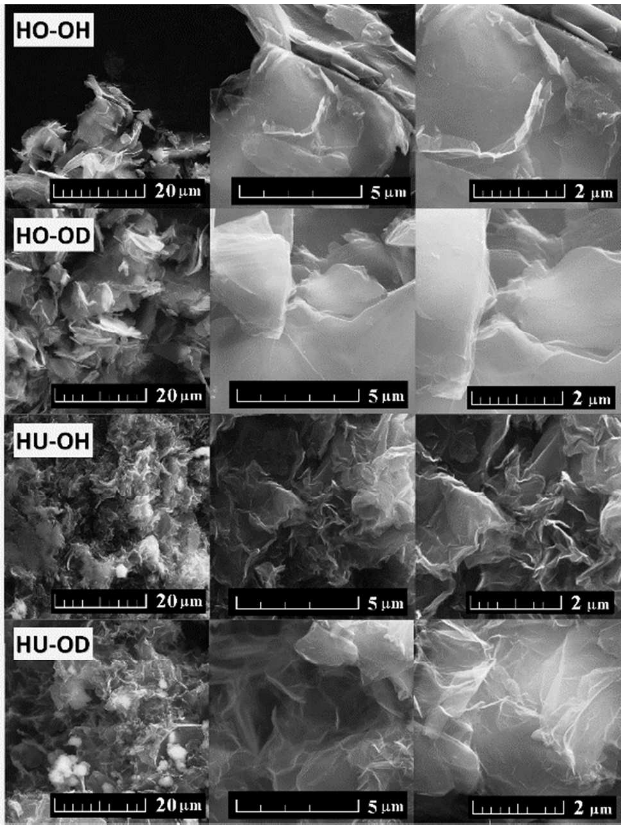

Fig. 1 The surface morphology of graphene at various magnifications.

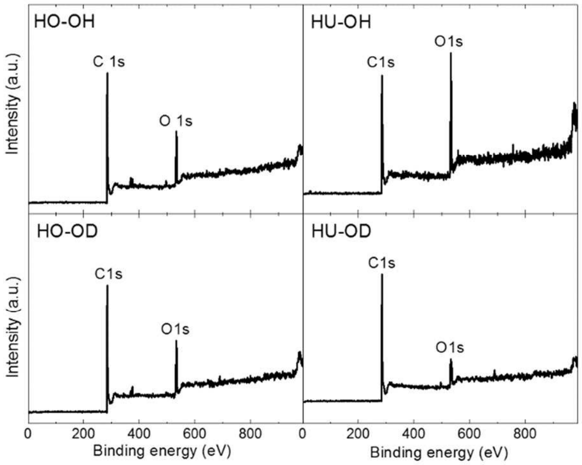

Fig. 2 Survey spectra of hydrogenated graphenes.

Table 3 The results of C 1s peak deconvolution with quantification of different carbon bonding states.

Sample	C=C	C-O/C-H	C-O	C=O	O-C=O	π-π*
HO-OH	54.5	16.7	6.5	10.2	0.9	11.1
HO-OD	51.2	17.9	8.7	9.4	5.6	7.2
HU-OH	42.5	15.3	12.5	13.8	4.4	11.6
HU-OD	49.4	15.9	5.2	9.2	4.0	16.2

The elemental composition was investigated using elemental combustion analysis. The results in atomic percent are summarized in **Table 4**. A slightly lower concentration of hydrogen observed in deuterated samples is caused by different molar mass of deuterium compared to hydrogen. The first indication of graphene hydrogenation originates from H/O ratio. Since the H/O ratio corresponding to various oxygen functional groups is always less or equal to unity (0.5 for carboxylic acids, 1for hydroxyl groups and 0 for other oxygen functional groups like epoxide and ketone), the value higher than 1 is a cler indication of C-H bonds formation. For the rough estimation of minimum hydrogen concentration in the form of C-H group we can use a simple subtraction of hydrogen and oxygen concentration. These results are also shown in **Table 4**. Let us note that the composition of the starting graphite oxides was 46.65 at.% C, 22.08 at.% H and 31.27 at.% O for HO-GO and 43.39 at.% C, 24.61 at.% H and 32.00 at.% O for HU-GO.

Table 4 Composition in at. % of reduced/hydrogenated graphene obtained by elemental combustion analysis. Right column shows a minimal concentration of C-H bonds obtained from $c_{(C-H)}$ = H – O.

Sample	N	C	H	O	(C-H)
HO-OH	0.06	58.78	21.24	19.93	1.31
HO-OD	0.08	58.78	21.81	22.77	-0.96
HU-OH	0.19	54.92	22.31	22.58	-0.27
HU-OD	0.14	64.10	15.99	19.77	-3.78

Another evidence of C-H bond formation can be obtained by FT-IR spectroscopy (**Figure 4**). The C-H band observed around 2920 cm^{-1} and 2850 cm^{-1} provides a clear evidence of graphene hydrogenation. However, FT-IR spectra are significantly influenced by high absorption of graphene and only very weak intensities of bands are usually observed. In addition to that we can see a broad vibration band of hydroxyl functional group at 3400 cm^{-1}. This band dominantly present in graphene originates from HO-GO precursor. Lower degree of reduction can be seen on HU-OH sample where an additional band corresponding to C=O functional groups can be seen at 1710 cm^{-1}. The vibration of graphene skeleton originating from C=C bands is clearly visible at 1630 cm^{-1}. The broad vibration band at 1380 cm^{-1} is related to the vibration of C-O bonds from remaining oxygen functional groups. For comparison, the FT-IR spectra of starting graphite oxides are shown in Supporting Information (**Figure SI2**).

Although all the above mentioned methods can give information about the presence of C-H, they cannot be used for exact quantitative determination of hydrogen concentration in the form of C-H bond. In order to resolve this problem, we used the combination of ERDA and RBS (**Figure 5**). The results of ERDA and RBS analysis of the starting graphite oxides are shown in Supporting Information (**Figure SI3**). Since ERDA is sensitive to light elements, it is very useful for the quantification of hydrogen and deuterium concentration. On the other hand RBS was used for heavier elements trace analysis.

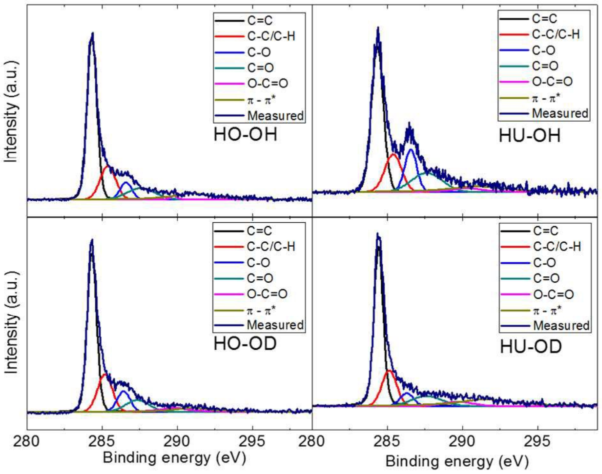

Fig. 3 High resolution XPS spectra of C 1s peak of hydrogenated graphenes with fit of various carbon bonding states.

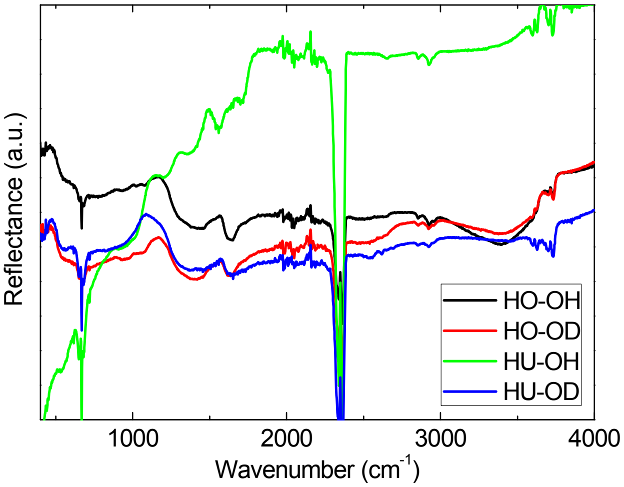

Fig. 4 FT-IR spectra of reduced graphene.

The use of deuterated solvents and reactants led to the formation of deuterium labeled hydrogenated graphene. Subsequent treatment of such material with normal hydrogen led to deuterium exchange in all acidic groups like hydroxyls or carboxylic groups. Only C-D bonds remained unchanged during this process and the exact determination of deuterium content yielded the extent of graphene hydrogenation/deuteration. The concentrations of hydrogen, deuterium, carbon and oxygen obtained by combination of ERDA and RBS methods are summarized in the **Table 5**. A higher degree of hydrogenation was observed for HO-OH and HO-OD samples. This is related to the different chemistry of HO-GO where more reactive functional groups like epoxides are present compared to HU-GO. These results are consistent with the data obtained by elemental combustion analysis showing a higher concentration of hydrogen in the form of C-H bond observed for the same samples.

Table 5 The concentration of carbon, oxygen, hydrogen and deuterium measured by RBS (O and C) and ERDA (H and D) in at.%.

Sample	C	O	H	D
HO-OH	73.4	18.1	6.5	0.0
HO-OD	71.3	12.6	9.3	6.8
HU-OH	73.2	12.9	13.9	0.0
HU-OD	72.3	14.9	9.5	3.3

The hydrogenated graphenes were further investigated using Raman spectroscopy. Two main peaks located at 1560 cm^{-1} and 1340 cm^{-1} were found in the observed Raman spectra (**Figure 6**). The peak located at 1560 cm^{-1} (G-band) is associated with the sp^2 hybridized carbon atoms within hexagonal graphene framework. The peak at 1340 cm^{-1} (D-band) is related to the carbon atoms with sp^3 hybridization originating from the remaining oxygen functional groups and defects in the graphene layer. In addition, a weak peak observed around 2690 cm^{-1} (2D-band) is associated with the number of layers. The intensities of D and G peaks are denoted as I_D and I_G, the ratio of their intensities corresponding to defects within the graphene structure. For the reduced/hydrogenated graphenes the following values were obtained: 1.28 for HU-OD, 1.10 for HU-OH, 1.03 for HO-OH and 1.04 for HO-OD. Higher degree of reduction and lower concentration of defects can be observed on samples prepared from HO-GO. This is in correlation with the composition of starting graphite oxide, where HU-GO contained higher concentration of carboxylic acids and ketone functional groups. These functional groups were formed on the edges of graphene sheets and/or they were linked to defects within the graphene framework.

In addition to chemical composition the measurement of resistivity was performed. The resistivity of graphene samples is strongly correlated to the degree of reduction and concentration of the remaining functional groups. The HO-OH and HO-OD exhibited the resistivity 1.42x10^{-2} Ω.cm^{-1} and 1.37x10^{-2} Ω.cm^{-1}, respectively, while for HU-OH and HU-OD the respecitve values 4.60 Ω.cm^{-1} and 1.88x10^{-1} Ω.cm^{-1} were attained. Samples with highest degree of reduction revealed a lower specific resistivity. A significant difference was also found between the samples originated from various graphite oxides. Higher resistivity observed for samples synthesized from HU-GO was related to the higher concentration of defects which was confirmed by Raman spectroscopy and by the higher concentration of oxygen functional groups.

In order to further investigate the remaining functional groups the measurement of inherent electrochemistry in phosphate buffer was performed. Significant differences in composition of the remaining oxygen functional groups between the hydrogenated graphenes were observed (**Figure 7**). The electrochemical data show that there is a significant difference in the reduction efficiency between graphene oxides prepared by chlorate chlorate (HO) and permanganate (HU) methods in terms of residual electrochemically reducible groups (epoxy, peroxy, aldehyde).[25]

The reduction of HO-OH and HO-OD started at -0.67 V and -0.57 V and reached the maximum at -1.28 V and -1.51 V, respectively. In the case of HU-OH the reduction started already at 0.13 V and culminated at -1.18 V. This result is in good agreement with other data obtained by XPS and FT-IR, where relatively high

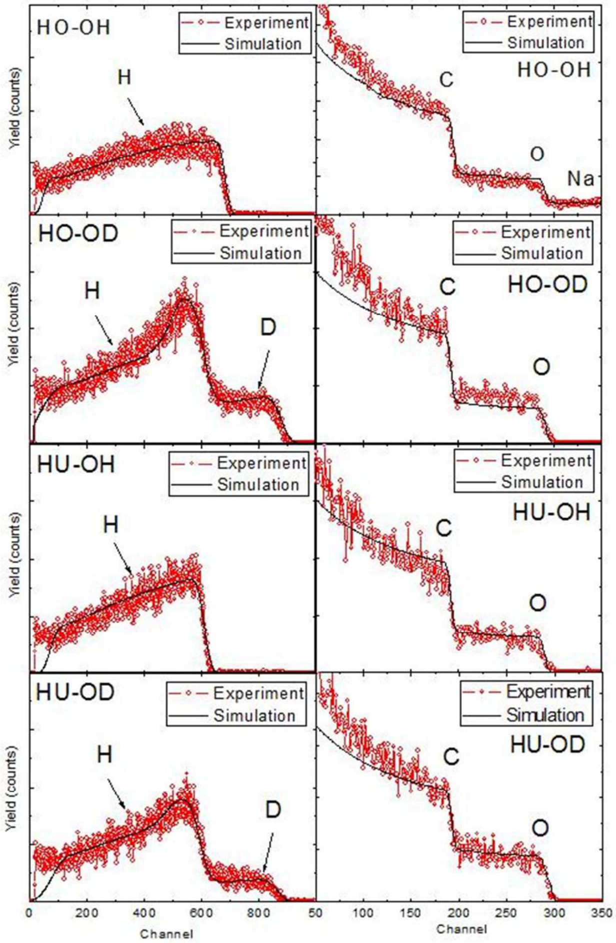

Fig. 5 ERDA (left) and RBS (right) spectra of hydrogenated graphenes.

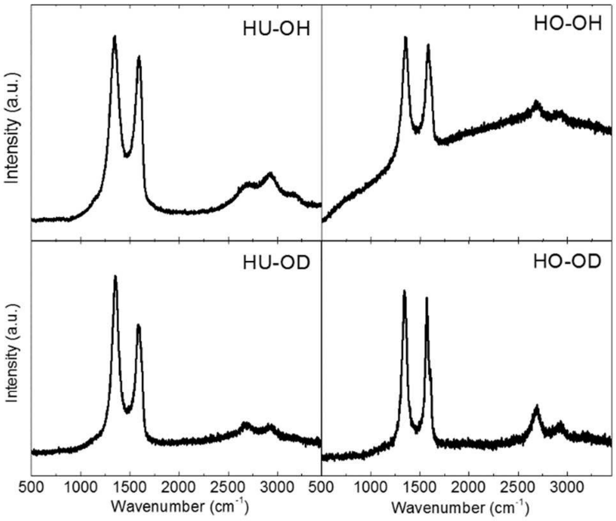

Fig. 6 Raman spectra of hydrogenated graphenes.

concentration of remaining oxygen functional groups was observed in comparison with the other samples. The HU-OD sample exhibited a significantly higher degree of reduction. As a result a weak reduction current was observed starting from -0.4 V and it is further increased at -1.16 V. However, no obvious reduction current maximum was observed for this sample.

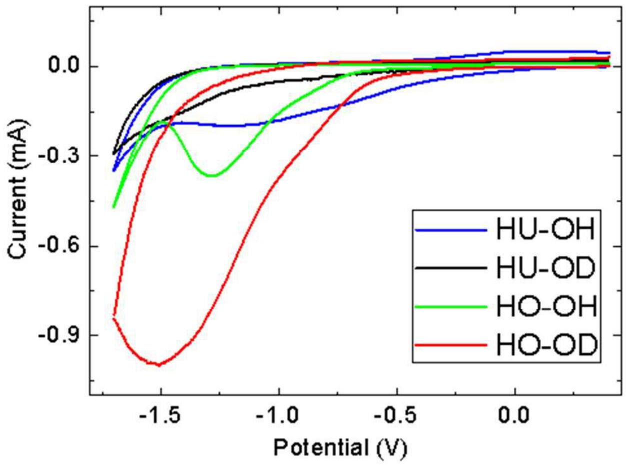

Fig. 7 The inherent electrochemistry of hydrogenated graphenes. (50 mM PBS, pH = 7.0, Scan rate = 0.1 V/s).

Conclusions

The reduction with simultaneous hydrogenation of two different graphite oxides prepared by chlorate and permanganate routes was performed using aluminum powder in alkaline environment. The hydrogenation of the reduced graphene was proved using FT-IR spectroscopy and elemental combustion analysis. Deuterium labeled graphenes were prepared using deuterium oxide and deuterated sodium hydroxide. The nuclear analytical methods like RBS and ERDA were used for exact quantification of deuterium concentration within hydrogenated graphenes. Using a combination of these methods we were able to measure the exact degree of hydrogenation. We showed that both graphene oxides prepared by permanganate and chlorate route can be efficiently reduced and hydrogenated. Obtained results confirmed a successful synthesis of highly hydrogenated graphenes as well as the viability of deuterium labeling technique as a highly efficient tool for the control hydrogenated graphene produced both in laboratory and industrial scale.

Notes and references

[a] *Institute of Chemical Technology, Department of Inorganic Chemistry, 166 28 Prague 6, Czech Republic, E-mail:zdenek.sofer@vscht.cz; Fax: +420 22431-0422*
[b] *Division of Chemistry & Biological Chemistry, School of Physical and Mathematical Sciences, Nanyang Technological University, Singapore, 637371, Singapore. E-mail: pumera@ntu.edu.sg; Fax: +65 6791-1961*
[c] *Institute of Nuclear Physics AS CR, v.v.i., Husinec - Řež, 130, 250 68 Řež, Czech Republic, E-mail:mackova@ujf.cas.cz; Fax: +420 220941130*
[d] *Department of Physics, Faculty of Science, J.E. Purkinje University, Ceske mladeze 8, 400 96 Usti nad Labem, Czech Republic*

Acknowledgements

The project was supported by Czech science foundation (Project No. 15-09001S) and by specific university research (MSMT no. 20/2015). RBS and ERDA analysis was realized at CANAM (Center of Accelerators and Nuclear Analytical Methods) LM 2011019. A.M. and R.M. were supported by the project P108/12/G108.

References

1. A. K. Geim and K. S. Novoselov, *Nat. Mater.*, 2007, **6**, 183-191.
2. R. R. Nair, W. Ren, R. Jalil, I. Riaz, V. G. Kravets, L. Britnell, P. Blake, F. Schedin, A. S. Mayorov, S. Yuan, M. I. Katsnelson, H.-M. Cheng, W. Strupinski, L. G. Bulusheva, A. V. Okotrub, I. V. Grigorieva, A. N. Grigorenko, K. S. Novoselov and A. K. Geim, *Small*, 2010, **6**, 2877-2884.
3. O. Jankovský, P. Šimek, K. Klímová, D. Sedmidubský, S. Matějková, M. Pumera and Z. Sofer, *Nanoscale*, 2014, **6**, 6065-6074.
4. O. Jankovský, P. Šimek, D. Sedmidubský, S. Matějková, Z. Janoušek, F. Šembera, M. Pumera and Z. Sofer, *RSC Advances*, 2014, **4**, 1378-1387.
5. K.-J. Jeon, Z. Lee, E. Pollak, L. Moreschini, A. Bostwick, C.-M. Park, R. Mendelsberg, V. Radmilovic, R. Kostecki, T. J. Richardson and E. Rotenberg, *ACS Nano*, 2011, **5**, 1042-1046.
6. M. Pumera and C. H. A. Wong, *Chem. Soc. Rev.*, 2013, **42**, 5987-5995.
7. J. O. Sofo, A. S. Chaudhari and G. D. Barber, *Physical Review B*, 2007, **75**, 153401.
8. R. A. Schäfer, J. M. Englert, P. Wehrfritz, W. Bauer, F. Hauke, T. Seyller and A. Hirsch, *Angewandte Chemie International Edition*, 2013, **52**, 754-757.
9. A. Y. S. Eng, H. L. Poh, F. Šaněk, M. Maryško, S. Matějková, Z. Sofer and M. Pumera, *ACS Nano*, 2013, **7**, 5930-5939.
10. Z. Yang, Y. Sun, L. B. Alemany, T. N. Narayanan and W. E. Billups, *J. Am. Chem. Soc.*, 2012, **134**, 18689-18694.
11. Z. Luo, T. Yu, K.-j. Kim, Z. Ni, Y. You, S. Lim, Z. Shen, S. Wang and J. Lin, *ACS Nano*, 2009, **3**, 1781-1788.
12. H. L. Poh, F. Sanek, Z. Sofer and M. Pumera, *Nanoscale*, 2012, **4**, 7006-7011.
13. Z.-J. Fan, W. Kai, J. Yan, T. Wei, L.-J. Zhi, J. Feng, Y.-m. Ren, L.-P. Song and F. Wei, *ACS Nano*, 2010, **5**, 191-198.
14. X. Mei and J. Ouyang, *Carbon*, 2011, **49**, 5389-5397.
15. Z. Sofer, O. Jankovský, P. Šimek, L. Soferová, D. Sedmidubský and M. Pumera, *Nanoscale*, 2014, **6**, 2153-2160.
16. Z. Fan, K. Wang, T. Wei, J. Yan, L. Song and B. Shao, *Carbon*, 2010, **48**, 1686-1689.
17. O. Jankovský, P. Šimek, D. Sedmidubský, Š. Huber, M. Pumera and Z. Sofer, *RSC Advances*, 2014, **4**, 7418-7424.
18. U. Hofmann and A. Frenzel, *Kolloid-Z.*, 1934, **68**, 149–151.
19. W. Hummers and R. Offeman, *J. Am. Chem. Soc.*, 1958, **80**, 1339–1339.
20. C. H. A. Wong, O. Jankovský, Z. Sofer and M. Pumera, *Carbon*, 2014, **77**, 508-517.
21. J. Saarilahti and E. Rauhala, *Nucl. Instrum. Meth. B*, 1992, **64**, 734.
22. M. Mayer, SIMNRA version 6.06, Max-Planck-Institut fur Plasmaphysik, Garching, Germany, 2011. Available at: http://home.rzg.mpg.de/~mam/Download.html.
22. IBANDL, http://www-nds.iaea.org/ibandl/.
23. L. J. van der Pauw, *Philips Tech. Rev.*, 1958, **20**, 220–224.
24. E.L.K. Chng, M. Pumera, *Chem. Asian J.*, 2011, **6**, 2899-2901.